Microdroplet Coalescences at Microchannel Junctions with Different Collision Angles

Kai Wang, Yangcheng Lu, Lu Yang, and Guangsheng Luo
Dept. of Chemical Engineering, The State Key Laboratory of Chemical Engineering, Tsinghua University, Beijing 100084, People's Republic of China

DOI 10.1002/aic.13825
Published online May 11, 2012 in Wiley Online Library (wileyonlinelibrary.com).

Microdroplet coalescence mechanism is very important for the miniaturization of multiphase chemical processes with microstructured devices. Using three working systems with different physical properties, this article presents an experimental study on the fluid dynamics of microdroplet coalescence at different microchannel junctions. The critical capillary number to distinguish coalescence or noncoalescence of microdroplet is investigated and its variations with droplet size, collision angle, and physical properties are analyzed with two important parameters – the film drainage time and droplet contact time. Experimental results indicate that microdroplet coalescence can be enhanced by reducing the droplet collision angle. The differences of microdroplet coalescences in confined microchannels and free-flowing spaces are provided with the analysis of critical capillary number. A model equation is proposed to predict the critical capillary numbers in this study, which may provide valuable information for the design and development of new microstructured chemical device. © 2012 American Institute of Chemical Engineers *AIChE J,* 59: 643–649, 2013
Keywords: microdroplet, microchannel junction, coalescence, critical capillary number, film drainage theory

Introduction

During recent years, microstructured chemical devices have displayed essential roles in chemical engineering science and technology researches with a wide variety of applications including medicine,[1] food,[2] material,[3] and energy.[4] Precisely controlled droplets and bubbles on the micrometer scale with size distributions less than 5% have been successfully generated in the T-junction,[5,6] flow focusing,[7] coaxial,[8,9] and some other kinds of microfluidic devices.[10–12] These microscaled dispersed fluid particles can be used to enhance and control the heat and mass-transfer processes in many areas, such as organic synthesis,[13] medicine delivery,[14] particle preparation,[15] gas absorption,[16] solvent extraction,[17] etc.

Besides the generation of microdroplets and microbubbles, the coalescence of microdroplets and microbubbles is also an important issue in the application of microstructured chemical technology, especially for the miniaturization of multiphase reaction and separation processes. Microdroplet coalescence is not only a required process to realize phase separation in common chemical engineering process but also becomes an effective method to make reagent mixing and induce chemical reaction with small volume droplets as carriers in microchannel device.[18–20] Several methods have been developed to promote microdroplet coalescence, including active ways with energy input[21–23] and passive ways depending on the device structure or wetting properties.[24–26] Although these methods worked well in some applications,[20,27,28] fundamental studies on the fluid dynamics of microdroplet coalescence are still limited. It is still highly required to understand the coalescence mechanism of microscaled droplets for their application in large-scaled chemical process.

Previous fluid dynamic studies focused more on the millimeter-scaled droplets coalescing in the free-flowing space. One of the most famous theories for droplet coalescence is the film drainage theory,[29] characterizing the coalescence process with two important parameters: the "droplet contact time" and "film drainage time."[30] To achieve coalescence, two droplets need to approach each other and drain off the continuous phase fluid between their surfaces until the van der Waals forces lead to fusion.[31,32] Otherwise, elastic-like collision of droplets will take place. Besides the film drainage theory, some other studies characterize the droplet coalescence process with stress analysis. For example, in the study of head-on droplet coalescence process, a controlling parameter – the capillary number ($Ca = \mu_C u/\gamma$, where μ_C is the continuous phase viscosity, u is the flow velocity, and γ is the interfacial tension) describing the relative magnitude of viscous stress and interfacial tension – is proposed.[33] Leal and coworkers[34,35] have demonstrated that the head-on droplet coalescence only occurs as the capillary number below a critical value – the critical capillary number (Ca^*).

Comparing with the large droplets in common chemical device, the microdroplets in microsturctured device have some unique characters. First of all, the size of the microdroplet is much smaller than the millimeter-scaled droplets, which brings good mass and heat transport performances. Second, unlike the droplets flowing in the free spaces, such

Correspondence concerning this article should be addressed to K. Wang at kaiwang@tsinghua.edu.cn or G. S. Luo at gsluo@tsinghua.edu.cn.

© 2012 American Institute of Chemical Engineers

as extraction columns or stirring reactors, most of the microdroplets run in confined microchannels. Third, the flow field in microstructured device is regular and easily controlled laminar flow, which is very different from the turbulent flow in large columns and vessels. Considering these special characters and the mechanism requirement from microstructured chemical device applications, the basic study on the fluid dynamics of microdroplet coalescence is therefore highly required. In recent years, Christopher et al.[36] gave an experimental research on the liquid-plug collisions at T-shaped microchannel junction. In their experiment, the critical capillary number was also observed for the occurrence of plug coalescence. In our pervious work, the microbubble collisions at different T-shaped microchannel junctions with different channel widths were carefully investigated and the characterized film drainage time and bubble contact time were concluded as the main factors determining microbubble coalescence.[37]

In this work, we give a further research on the microdroplet collisions at T-shaped and Y-shaped microchannel junctions to make in-depth analysis on the fluid dynamics of microdroplet coalescence based on the variation of the critical capillary number for microdroplet coalescence. Experiments are made with different working systems, and semi-empirical equations for the droplet contact time and the film drainage time are established based on the experiment results. Coalescence enhancement method based on the increase of droplet contact time is proposed with the reduction of the droplet collision angle. The relation of droplet contact time and film drainage time with the critical capillary number is discussed and a model equation is established to calculate the critical capillary numbers in this study.

Experiment

Schematic figures of the microchannel devices used in the experiment are shown in Figure 1 with designed structural parameters. In each microdevice, there are two flow-focusing droplet generation structures. The lengths of the orifices in all these generation structures are 0.5 mm and their heights and widths are both 0.3 mm ($w = h = 0.3$ mm). The main channels in these devices given by thick lines in Figure 1 have square sections, whose widths and height are both 0.6 mm ($W = H = 0.6$ mm). The meeting junctions of the microchannels are fabricated as T-shape and Y-shape with

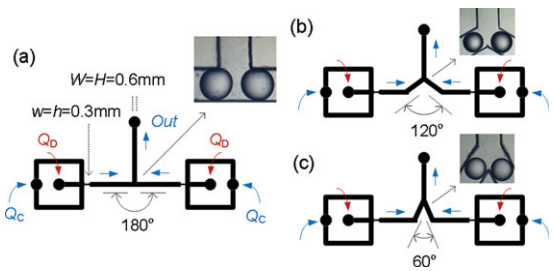

Figure 1. Schematics of the microchannel devices used in this study and pictures of the meeting junctions.

The main channels are shown as thick lines and the orifices are given as thinner lines. The inlets and outlets of two-phase fluids as well as their flow directions are indicated with arrows. (a) $\theta = 180°$; (b) $\theta = 120°$; (c) $\theta = 60°$. [Color figure can be viewed in the online issue, which is available at wileyonlinelibrary.com.]

Table 1. Physical Property of the Three Working Systems (27°C)

Systems	Viscosities of Water Phase μ_D (MPa s)	Viscosities of Alcohol Phase μ_C (MPa s)	Interfacial Tensions γ (mN/m)
Water/pentanol	0.92 ± 0.02	3.13 ± 0.05	4.15 ± 0.11
Water/octanol	0.85 ± 0.01	6.65 ± 0.04	7.55 ± 0.09
Water/decanol	0.90 ± 0.02	10.74 ± 0.08	8.02 ± 0.25

collision angles (θ) of 180°, 120°, and 60° in the middle of these devices. Microdroplet collisions are performed at these microchannel junctions during the experiment. The downstream channels of the meeting junctions have same cross sections as the upstream channels. These microchannel devices were fabricated on polymethyl methacrylate (PMMA) plates with end mills and sealed to chips by a high-pressure thermal sealing machine (A274, Techson) at 75°C, 0.4 MPa. The fabrication errors were about 0.02 mm for the microstructures. The inlets and outlets of two-phase fluids were drilled on top of these chips, connected with Teflon pipes. Only water and ethanol were used in the fabrication processes to avoid contamination.

Water/alcohol two-phase systems are commonly used in chemical engineering processes and they can form water-in-oil droplets without surfactant in PMMA microchannels.[38,39] In this study, water/pentanol, water/octanol, and water/decanol (Sinopharm Chemical Reagent) were selected as working systems. The two-phase fluids were premixed together before experiment to ensure no mass transfer occurring within the collision processes. Physical properties of these working systems measured with an Ubbelohde viscometer and a commercial tensiometer (OCAH200, DataPhysics Instruments GmbH) at 27°C are given in Table 1.

Feeding of both phase fluids were driven by syringe pumps (TS2-60, Longer) and controlled consistently in both generators of the microchannel devices to make equal-sized microdroplets. Before running each experiment, the alcohol phase was first pumped into the microchannel device to wet the channel wall. After changing any operating condition, at least 5-min time was allowed for the two-phase flow reaching stable state. The flowrates of dispersed phase (Q_D) were controlled from 1 to 70 μL/min and the flowrates of continuous phase (Q_C) were varied from 10 to 260 μL/min in the experiment. Microdroplet collisions were made at the meeting junctions and recorded by a high speed camera (PL-B742F, PixeLINK) on an optical microscope (Olympus) at frame rate of 220 frames per second. The droplet diameters were measured from the recorded pictures and the small measurement error only came from the picture resolution – 0.005 mm/pixel; 0.01 mm (2 pixels) was the biggest measurement error for the droplet diameter. To analyze the movement of droplet mass center in their collision processes, a self-made computer program is made to find the two-dimensional mass center of droplet in recorded pictures ($x_m = \Sigma m_i x_i / \Sigma m_i$, where x_i is the position of a pixel point and m_i is a number to identify the pixel point in droplet. $m_i = 1$ in droplet and $m_i = 0$ at the outside). The film drainage time and the droplet contact time were also counted from the frames of recorded videos. The film drainage time is defined as the time interval from droplet contact to droplet fusing, and the droplet contact time is the time interval from droplet contact to droplet separation. The time measurement error is just the time interval between adjacent frames – 0.0045 s.

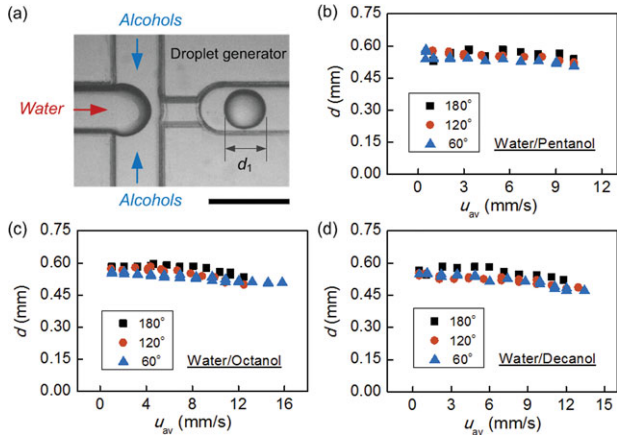

Figure 2. Microdroplet generation in a flow-focusing generator and the average droplet diameters in experiment.

u_{av} is the average velocity of two-phase fluids, defined as $u_{av}=(Q_C + Q_D)/WH$. (a) A picture of microdroplet and the flow-focusing generator; (b) the average droplet diameters in water/pentanol experiment; (c) water/octanol experiment; (d) water/decanol system. The scale bar is 1 mm. [Color figure can be viewed in the online issue, which is available at wileyonlinelibrary.com.]

To eliminate the time difference between the arrivals of two droplets at the meeting junction, the synchronization of the generators was strictly controlled and all the results in this article were chosen from the tests that collisions started at the center of the meeting junctions. Several tests are repeated for one operating condition to give parallel experimental results.

Result and Discussion

Collisions of microdroplets

The microdroplet generation in a flow-focusing generator is shown in Figure 2a. We observed that all the microdroplets generated in the same generator had small size distributions with relative diameter deviations less than 3%. The average diameters of droplets from two opposite generators, $d = (d_1 + d_2)/2$ (d_1 and d_2 are diameters of droplets from different generators in one experimental device), at different operating conditions are ranging from 0.47 to 0.58 mm as shown in Figures 2b–d. The relative deviations of d_1 and d_2 coming from the fabrication errors (~0.02 mm) in microchannel devices were less than 6% in all the experiments. Figure 2 shows the droplet diameters are close to the channel width ($d > 0.8\ W$); therefore, the droplet flows were confined by the channel walls.

The microdroplets moved regularly one after the other without any contact in the upstream channels. Collisions only took place at the junction centers. The droplet collision processes were well repeated in each operating condition and the collision results indicated that all the three working systems displayed coalescence phenomena at very low average velocity of two-phase fluids ($u_{av} = (Q_C + Q_D)/WH$). Although at high average velocities, the two droplets separated at last. Some representative photographs from recorded videos are shown in Figure 3, which shows coalesced droplets on the left-hand side and noncoalescence droplets on the right-hand side. In confined microchannels, the droplet collision process is less of randomness, which can be clearly disintegrated to several stages. A scheme diagram for these stages is shown in Figure 4. For the coalesced microdroplets, they flow from upstream microchannels and contact with each other at first. Then, they block the channel section and begin to squeeze with each other with the narrowing of microchannel junction. A liquid film forms between their contacting surfaces preventing droplet fusion and the film area increases with the two droplets coming closer. At the same time, the film thickness reduces with the proceeding of draining process. When the film thickness reaches to a critical value as the van der Waals forces on droplet surfaces start to work, droplet fusion takes place instantly. For the noncoalescence microdroplets, they keep squeezing with each other in the whole collision process. Even reaching the strongest droplet deformation, the film drainage process has not finished. Because of the droplet surface deformation, the interfacial energy increases with the squeezing of droplets. When this energy reaches its highest value, the squeezing process comes to the end and the release of stored interfacial energy causes quick droplet separation. The noncoalesced droplets traveled downstream one after the other at last.

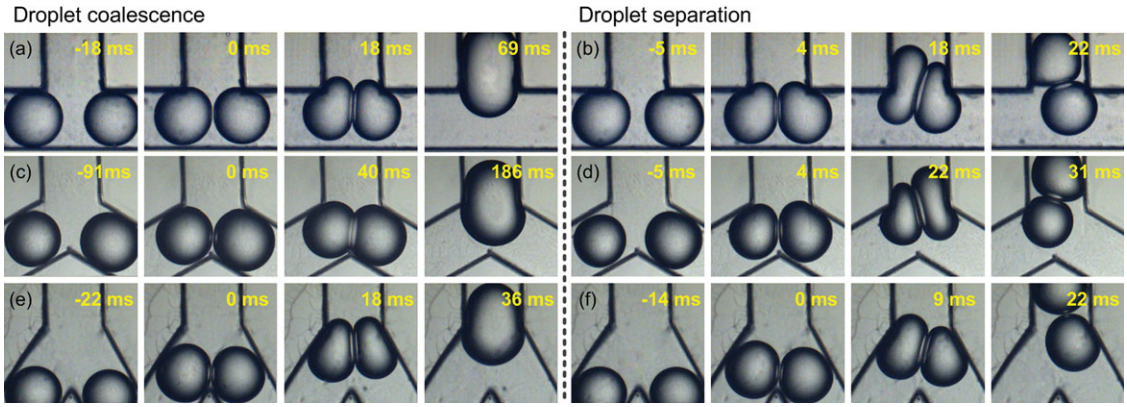

Figure 3. Time sequences showing the behaviors of microdroplets at different microchannel junctions: contact, squeezing, coalescence, or separation.

The zero time in these pictures is defined as the moment droplets start to contact. (a,b) Experiments at collision angle 180° with water droplets in pentanol. $u_{av} = 3.6$ mm/s in Figure 3a; $u_{av} = 10.1$ mm/s in Figure 3b. (c,d) Experiments at collision angle 120° with water droplets in decanol. $u_{av} = 1.1$ mm/s in Figure 3c; $u_{av} = 9.7$ mm/s in Figure 3d. (e,f) Experiments at collision angle 60° with water droplets in octanol. $u_{av} = 6.9$ mm/s in Figure 3e; $u_{av} = 14.6$ mm/s in Figure 3f. [Color figure can be viewed in the online issue, which is available at wileyonlinelibrary.com.]

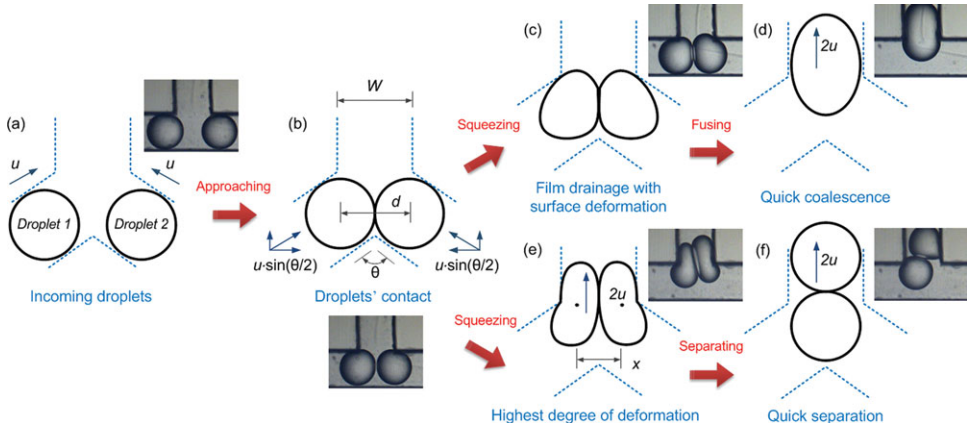

Figure 4. A scheme diagram of the developing stages and some characterized parameters in the microdroplet collision processes.

(a) Droplet flow; (b) droplet contact; (c) squeezing; (d) fused droplet; (e) strongest deformation; (f) separated droplets. [Color figure can be viewed in the online issue, which is available at wileyonlinelibrary.com.]

Critical capillary number

Repeated tests for one operating condition were made several times and droplet coalescence was observed in all the parallel tests at very low average velocities. While at higher average velocities, the droplets were separated with each other in all repeated tests. Between the absolute coalescence and noncoalescence regions, a narrow transition region existed, where both droplet coalescence and noncoalescence occurred. The coalescence and noncoalescence regions are clearly distinguished in the experiment due to the narrow operating region of transition state; therefore, the microdroplet coalescence processes can be strictly controlled in microchannels. This controllability is attributed to the regular two-phase flow in the microstructured device. The center of the transition region represents the critical condition for the occurring of microdroplet coalescence. According to some previous researches,[33–36] droplet coalescence can be determined by the critical capillary number lower than which coalescence takes place. The critical capillary numbers of microdroplet coalescences in this work's experiment are given in Figure 5 showing the critical capillary number increases with the decrease of collision angle. This result represents that it is benefit for microdroplet coalescence at higher flowrate in the Y-shaped microchannel junction. Therefore, the microdroplet coalescence can be enhanced by decreasing the droplet collision angle. The critical capillary numbers varied from 0.0026 to 0.014 in this work's experiment and Figure 5 shows that these critical capillary numbers are different for different working systems.

Film drainage time and droplet contact time

To give a more in-depth understanding of the mechanism of microdroplet coalescence, the droplet collisions are analyzed in more detail with the film drainage theory. In the experiment, the time interval from droplet contact to fusion gives the film drainage time and the time interval from their contact to complete separation shows the droplet contact time provided by the two-phase flow at microchannel junction. Figure 6 exhibits the average film drainage time, the average droplet contact time, and their distributions of parallel tests with color dots and error bars. We can find the film drainage time is on the range of 10^{-2} s and changes little with the variation of collision angle and average velocity. This result accords with the viscous forced controlled film drainage process of deformable fluid particles with fully mobile interfaces described in the review article of Liao and Lucas.[29] In the studies of multiphase flow at micrometer scale, the viscous force has been proved as one of the main forces affecting microflows[10] and our previous work has demonstrated that the viscosity of continuous phase is very important for the determination of microbubble coalescence in microchannels.[37] Some other reports have also introduced that this fully mobile interfaces commonly exist in the liquid–liquid dispersed systems without surfactant and mass-transfer processes,[30,31] the same as the working systems in this study. According to the theoretical model provided by Liao and Lucas,[29] the viscosity force controlled the film drainage time for the deformable fluid particle with fully mobile interface proportional to the viscosity of continuous phase, droplet size, interfacial tension, and variation of film thickness between droplet surfaces, as shown in Eq. 1

$$t_{dr} \sim \frac{\mu_C d}{\gamma} \ln\left(\frac{h_i}{h_f}\right) \tag{1}$$

where h_i is the initial film thickness and h_f is the final film thickness before fusion. According to a previous article of Yeo

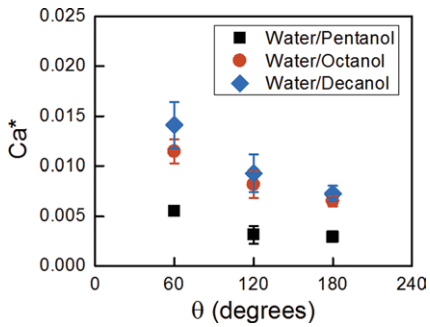

Figure 5. The critical capillary numbers of different working systems. The error bars give the transition regions, where both droplet coalescence and noncoalescence take place.

[Color figure can be viewed in the online issue, which is available at wileyonlinelibrary.com.]

et al.,[40] the most important parameter affecting h_i and h_f is the viscosity ratio of two-phase fluids and some other experimental studies have demonstrated that the two-phase viscosity ratio is an important parameter for the critical capillary number of microdroplet coalescence.[36,41] Based on this analysis, the effect of film thickness variation on the film drainage time is expressed as a dimensionless formula of two-phase viscosity ratio in this study

$$\ln\left(\frac{h_i}{h_f}\right) \sim p'\left(\frac{\mu_C}{\mu_D}\right)^k \tag{2}$$

and a semiempirical equation is built for the film drainage time considering its main influencing factors, shown as

$$t_{dr} = p\frac{\mu_C d}{\gamma}\left(\frac{\mu_C}{\mu_D}\right)^k \tag{3}$$

where p, p', and k are dimensionless parameters. Correlated from the experimental results, the equation of t_{dr} for different working systems are given in Table 2 and shown as the dash lines in Figure 6 ($P = 304 \pm 31$ and $k = -0.750 \pm 0.061$ in 95% confidence intervals of t_{dr}). Comparing with the millimeter-scaled droplet coalescence processes with similar physical properties (t_{dr}: 0.1–10 s),[30,31] the film drainage time is much shorter at micrometer scale (t_{dr}: 10^{-2} s). Together with the compelled collision in confined microchannel, fast film drainage process is easier to realize for microdroplet, which is different from the common multiphase processes in extraction columns or stirring reactors.

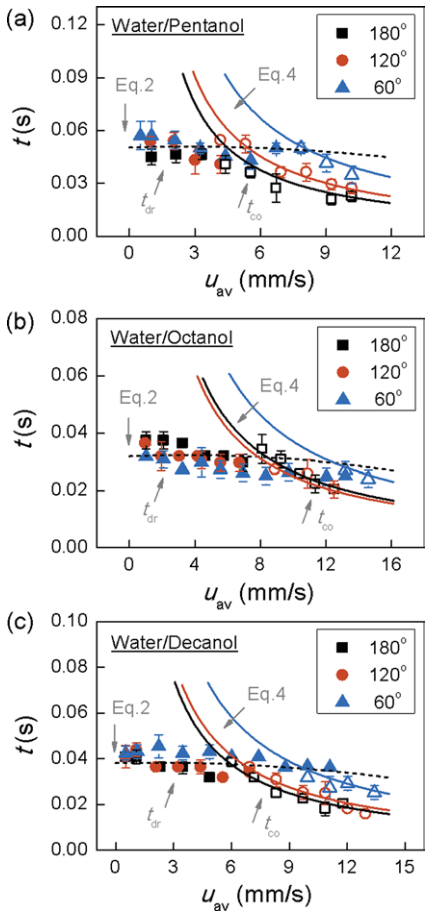

Figure 6. The droplet contact time and the film drainage time.

The solid symbols show the average film drainage time of coalesced droplets (t_{dr}) and the open symbols give the average contact time from separated droplets (t_{co}). The error bars are the time distributions in parallel experiments. The solid lines give the calculated droplet contact time from Eq. 4 and the dashed lines show the calculated film drainage time from Eq. 3. (a) Water/pentanol system; (b) water/octanol system; (c) water/decanol system. [Color figure can be viewed in the online issue, which is available at wileyonlinelibrary.com.]

Table 2. Formulas for the Film Drainage Time and the Droplet Contact Time

Film Drainage Time t_{dr}	Droplet Contact Time t_{co}
$304\frac{\mu_C d}{\gamma}\left(\frac{\mu_C}{\mu_D}\right)^{-0.750}$	$\frac{d - 0.315\ (\text{mm})}{u_{av}\sin(\theta/2)}$
$\left(10^{-4}\text{s} < \frac{\mu_C d}{\gamma} < 10^{-3}\text{s}, 0.07 < \frac{\mu_D}{\mu_C} < 0.3\right)$	$(60^\circ \le \theta \le 180^\circ, u_{av} < 15\ \text{mm/s})$

The hollow signals in Figure 6 are the average droplet contact time at microchannel junctions. The droplet contact time is also on the range of 10^{-2} s but reduces with the increases of the average velocity and droplet collision angle, representing that it is mainly determined by the two-phase flow at microchannel junctions. For the noncoalesced microdroplets in the experiment, the droplet contact time is lower than the calculated film drainage time from Eq. 3, as shown in Figure 6. This is the main reason for the unfinished film drainage process. The droplet contact time is modeled from the movement of droplet mass centers in this study. As shown in Figure 4, the distance between droplet mass centers on the horizontal axis would change from d to x with the squeezing of droplets, where x is the shortest horizontal distance between droplet mass centers in the collision process. In this process, the relative horizontal velocity of droplets reduces from $2u_{av}\sin(\theta/2)$ to zero (Figure 4b–e). After reaching the highest degree of droplet deformation, the droplets separate with each other quickly (Figure 4ef). We observed that the droplet separation time was too short (less than the time resolution of our camera, 0.0045 s, much shorter than the time interval of droplet squeezing process) to be considered from the experiment; therefore, the droplet contact time is estimated by the squeezing process only. The mass center distances of microdroplets at their contacting moment and the highest deformed moment shown in Figures 4b,e were measured with our computer program. Based on the variation of the microdroplet mass center distance with the experimental time, the average relative velocity of droplets in their squeezing process is assumed as $u_{av}\sin(\theta/2)$ in this study, half of the relative velocity in the upstream microchannels. Using the totally moving distance of droplet mass centers and their average relative velocity, the droplet contact time is calculated by the following equation (Eq. 4)

$$t_{co} = \frac{d - x}{u_{av}\sin(\theta/2)} \tag{4}$$

Measured from recorded videos with the self-made computer program, x is identified as 0.315 ($\pm$0.009) mm, 5% higher than $W/2$. Comparing with the experimental data in Figure 6, the lines of calculated droplet contact time fit well with the experimental results. Figure 6 shows that the film drainage time is lower than the calculated droplet contact time for

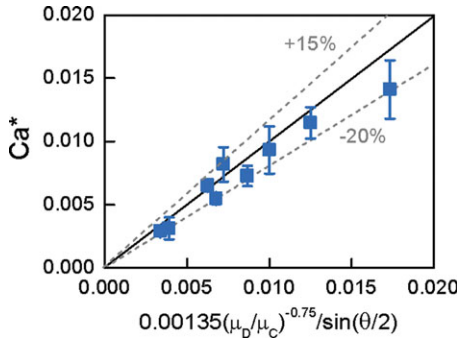

Figure 7. The relation of viscosity ratio, collision angle, and the critical capillary number.

The error bars show the transition regions where both droplet coalescence and separation occurred. The dashed lines give the fitting errors of Eq. 7. [Color figure can be viewed in the online issue, which is available at wileyonlinelibrary.com.]

coalesced microdroplets, which means the droplet contact time provided by the two-phase flow at the microchannel junctions is large enough to complete the film drainage process in those experiments. Reducing the droplet collision angle can increase the droplet contact time, which is benefit for the occurrence of microdroplet coalescence.

Quantification of the critical capillary number

Figure 6 illustrates that the calculated film drainage time and droplet contact time have intersections, representing the critical condition for microdroplet coalescence. When the droplet contact time equals to the film drainage time, Eq. 5 can be given

$$t_{dr} = p\frac{\mu_C d}{\gamma}\left(\frac{\mu_C}{\mu_D}\right)^k = t_{co} = \frac{d-x}{u_{av}\sin(\theta/2)} \tag{5}$$

According to Eq. 5, the critical capillary number for droplet coalescence is

$$Ca^* = \frac{\mu_C u_{av}}{\gamma} = \frac{1}{p}\left(1-\frac{x}{d}\right)\left(\frac{\mu_D}{\mu_C}\right)^k \cdot \frac{1}{\sin(\theta/2)} \tag{6}$$

Equation 6 shows that the critical capillary number has a linear relation with $1/\sin(\theta/2)$, hence, reducing droplet collision angle can enlarge the available operating region of microdroplet coalescence. For the confined microdroplets in this work ($d > 80\%\ W$), the ratio of x/d changed little ($x/d = 0.59 \pm 0.05$); therefore, Eq. 6 can be simplified as

$$Ca^* = 0.00135\left(\frac{\mu_D}{\mu_C}\right)^{-0.750}\frac{1}{\sin(\theta/2)}, \quad \text{where } 0.07 < \frac{\mu_D}{\mu_C} < 0.3, 60^\circ \le \theta \le 180^\circ \tag{7}$$

The measured critical capillary numbers given in Figure 7 fit well with the calculation results from Eq. 7.

Comparing with our experimental results for confined microdroplets at T-shaped microchannel junction and Christopher's results for microscaled liquid plugs,[36] ($Ca^* = 0.008$–0.004 at $\mu_D/\mu_C = 0.1$–0.3), we find that the critical capillary numbers for similar working systems are nearly the same, although the channel sizes are different (the channel width is 0.1 mm in Christopher's work) in different experiments. This comparison provides another evidence for the little effect of droplet size on the critical capillary number in confined microchannels. However, Hu et al.'s[41] studies have shown that the critical capillary numbers in the free-flowing spaces have power law dependence on droplet diameter ($Ca^* \sim d^{-0.82}$). Christopher et al.[36] found that the experimental critical capillary number for their 100-μm liquid plugs ($Ca^* \approx 0.02$) was similar as Hu's 100-μm droplets ($Ca^* = 0.022$) colliding in a predominantly extensional flow at a viscosity ratio of $\mu_D/\mu_C = 0.01$. They believed that the local dynamics near the droplet fusing points determined the coalescence process, although the nature of the global flow fields in the confined microchannels and free-flowing spaces were very different. According to the analysis of film drainage time and droplet contact time in this work, we believe that these closing critical capillary numbers may be a coincidence. The critical capillary number is determined by the film drainage time and the droplet contact time. The global flow in the collision space surely affects the droplet contact time, which cannot be neglected in the analysis of droplet coalescence process.

Conclusion

In summary, the microscaled droplet–droplet collision processes at three confined microchannel junctions are experimentally investigated with different water/alcohols' systems. Microdroplet coalescence processes can be well controlled attributing to the regular two-phase flow in microchannels. The experimental results indicate that the microdroplet coalescence is determined by two important time parameters – the film drainage time and droplet contact time. The film drainage time is mainly affected by the droplet size and physical properties of working systems, and the droplet contact time is a function of two-phase velocity and droplet collision angle, which can be easily changed to enhance the droplet coalescence process. When the contact time provided by the microchannel junction is larger than the film drainage time, droplet coalescence will take place. The critical capillary number is the special operating condition as the film drainage time equals to the droplet contact time. This critical capillary number is mainly affected by the viscosity ratio of two-phase fluids and the droplet collision angle, which can be simply represented by an equation of $Ca^* = 0.00135(\mu_D/\mu_C)^{-0.75}/\sin(\theta/2)$. This equation may provide valuable information for the design and operation of microstructured chemical devices.

In this work, the equal-sized microdroplet collision processes are discussed, which commonly exist in the microstructured chemical processes. However, not all the microdroplets to be coalesced in their applications must have equal sizes. The effect of droplet size difference on the microdroplet coalescence processes will be discussed in our further works. In addition, the studies concerning microdroplet coalescence mechanism with mass-transfer and surfactant adsorption processes will also be performed in our further researches using the experimental platform in this work to give a more comprehensive understanding of microdroplet coalescence process.

Acknowledgments

The authors acknowledge the support of the National Natural Science Foundation of China (21036002, 20111300342) and the Postdoctoral Science Foundation of China (20100480283, 201104095) for this work.

Literature Cited

1. Pihl J, Karlsson M, Chiu DT. Microfluidic technologies in drug discovery. *Drug Discov Today*. 2005;10:1377–1383.
2. Skurtys O, Aguilera JM. Applications of microfluidic devices in food engineering. *Food Biophys*. 2008;3:1–15.
3. Song YJ, Hormes J, Kumar C. Microfluidic synthesis of nanomaterials. *Small*. 2008;4:698–711.
4. Kjeang E, Djilali N, Sinton D. Microfluidic fuel cells: a review. *J Power Sources*. 2009;186:353–369.
5. Xu JH, Li SW, Tan J, Wang YJ, Luo GS. Preparation of highly monodisperse droplet in a T-junction microfluidic device. *AIChE J*. 2006;52:3005–3010.
6. Xu JH, Li S, Chen GG, Luo GS. Formation of monodisperse microbubbles in a microfluidic device. *AIChE J*. 2006;52:2254–2259.
7. Anna SL, Bontoux N, Stone HA. Formation of dispersions using "flow focusing" in microchannels. *Appl Phys Lett*. 2003;82:364–366.
8. Wang W, Xie R, Ju XJ, Luo T, Liu L, Weitz DA, Chu LY. Controllable microfluidic production of multicomponent multiple emulsions. *Lab Chip*. 2011;11:1587–1592.
9. Castro-Hernandez E, van Hoeve W, Lohse D, Gordillo JM. Microbubble generation in a co-flow device operated in a new regime. *Lab Chip*. 2011;11:2023–2029.
10. Zhao CX, Middelberg A. Two-phase microfluidic flows. *Chem Eng Sci*. 2011;66:1394–1411.
11. Wang K, Lu YC, Xu JH, Tan J, Luo GS. Generation of micromonodispersed droplets and bubbles in the capillary embedded T-junction microfluidic devices. *AIChE J*. 2011;57:299–306.
12. Wang K, Lu YC, Xu JH, Tan J, Luo GS. Liquid–liquid micro-dispersion in a double-pore T-shaped microfluidic device. *Microfluid Nanofluid*. 2009;6:557–564.
13. Su YH, Zhao YC, Jiao FJ, Chen GW, Yuan Q. The intensification of rapid reactions for multiphase systems in a microchannel reactor by packing microparticles. *AIChE J*. 2011;57:1409–1418.
14. Wei J, Ju XJ, Xie R, Mou CL, Lin X, Chu LY. Novel cationic pH-responsive poly (*N*,*N*-dimethylaminoethyl methacrylate) microcapsules prepared by a microfluidic technique. *J Colloid Interface Sci*. 2011;357:101–108.
15. Zhai Z, Chen Y, Wang YJ, Luo GS. Chiral separation performance of micrometer-sized monodispersed silica spheres with high protein loading. *Chirality*. 2009;21:760–768.
16. Tan J, Shao HW, Xu JH, Du L, Luo GS. Mixture absorption system of monoethanolamine triethylene glycol for CO_2 capture. *Ind Eng Chem Res*. 2011;50:3966–3976.
17. Choi YH, Song YS, Kim DH. Droplet-based microextraction in the aqueous two-phase system. *J Chromatogr A*. 2010;1217:3723–3728.
18. Sarrazin F, Prat L, Di Miceli N, Cristobal G, Link DR, Weitz DA. Mixing characterization inside microdroplets engineered on a microcoalescer. *Chem Eng Sci*. 2007;62:1042–1048.
19. Jin BJ, Kim YW, Lee Y, Yoo JY. Droplet merging in a straight microchannel using droplet size or viscosity difference. *J Micromech Microeng*. 2010;20:035003.
20. Frenz L, El Harrak A, Pauly M, Begin-Colin S, Griffiths AD, Baret JC. Droplet-based microreactors for the synthesis of magnetic iron oxide nanoparticles. *Angew Chem Int Ed. Engl*. 2008;47:6817–6820.
21. Li ZG, Ando K, Yu JQ, Liu AQ, Zhang JB, Ohl CD. Fast on-demand droplet fusion using transient cavitation bubbles. *Lab Chip*. 2011;11:1879–1885.
22. Zagnoni M, Baroud CN, Cooper JM. Electrically initiated upstream coalescence cascade of droplets in a microfluidic flow. *Phys Rev E*. 2009;80:463034.
23. Baroud CN, de Saint Vincent MR, Delville JP. An optical toolbox for total control of droplet microfluidics. *Lab Chip*. 2007;7:1029–1033.
24. Fidalgo LM, Abell C, Huck W. Surface-induced droplet fusion in microfluidic devices. *Lab Chip*. 2007;7:984–986.
25. Bremond N, Thiam AR, Bibette J. Decompressing emulsion droplets favors coalescence. *Phys Rev Lett*. 2008;100:245012.
26. Niu X, Gulati S, Edel JB, DeMello AJ. Pillar-induced droplet merging in microfluidic circuits. *Lab Chip*. 2008;8:1837–1841.
27. Liu K, Ding HJ, Chen Y, Zhao XZ. Droplet-based synthetic method using microflow focusing and droplet fusion. *Microfluid Nanofluid*. 2007;3:239–243.
28. Song H, Li HW, Munson MS, Van Ha TG, Ismagilov RF. On-chip titration of an anticoagulant argatroban and determination of the clotting time within whole blood or plasma using a plug-based microfluidic system. *Anal Chem*. 2006;78:4839–4849.
29. Liao YX, Lucas D. A literature review on mechanisms and models for the coalescence process of fluid particles. *Chem Eng Sci*. 2010;65:2851–2864.
30. Klaseboer E, Chevaillier JP, Gourdon C, Masbernat O. Film drainage between colliding drops at constant approach velocity: experiments and modeling. *J Colloid Interface Sci*. 2000;229:274–285.
31. Chevaillier JP, Klaseboer E, Masbernat O, Gourdon C. Effect of mass transfer on the film drainage between colliding drops. *J Colloid Interface Sci*. 2006;299:472–485.
32. Wu MM, Cubaud T, Ho CM. Scaling law in liquid drop coalescence driven by surface tension. *Phys Fluids*. 2004;16:L51–L54.
33. Yang H, Park CC, Hu YT, Leal LG. The coalescence of two equal-sized drops in a two-dimensional linear flow. *Phys Fluids*. 2001;13:1087–1106.
34. Yoon Y, Borrell M, Park CC, Leal LG. Viscosity ratio effects on the coalescence of two equal-sized drops in a two-dimensional linear flow. *J Fluid Mech*. 2005;525:355–379.
35. Borrell M, Yoon Y, Leal LG. Experimental analysis of the coalescence process via head-on collisions in a time-dependent flow. *Phys Fluids*. 2004;16:3945–3954.
36. Christopher GF, Bergstein J, End NB, Poon M, Nguyen C, Anna SL. Coalescence and splitting of confined droplets at microfluidic junctions. *Lab Chip*. 2009;9:1102–1109.
37. Yang L, Wang K, Tan J, Lu YC, Luo GS. Experimental study of microbubble coalescence in a T-junction microfluidic device. *Microfluid Nanofluid*. 2012;12:715–722.
38. Li SW, Xu HH, Wang YJ, Luo GS. Controllable preparation of nanoparticles by drops and plugs flow in a microchannel device. *Langmuir*. 2008;24:4194–4199.
39. Li SW, Xu JH, Wang YJ, Luo GS. Liquid–liquid two-phase flow in pore array microstructured devices for scaling-up of nanoparticle preparation. *AIChE J*. 2009;55:3041–3051.
40. Yeo LY, Matar OK, de Ortiz E, Hewitt GE. Film drainage between two surfactant-coated drops colliding at constant approach velocity. *J Colloid Interface Sci*. 2003;257:93–107.
41. Hu YT, Pine DJ, Leal LG. Drop deformation, breakup, and coalescence with compatibilizer. *Phys Fluids*. 2000;12:484–489.

Manuscript received Dec. 19, 2011, and revision received Apr. 8, 2012.